

# SENTINEL-1 DATA TIME SERIES TO SUPPORT FOREST POLICE IN HARVESTINGS DETECTION

De Petris S.<sup>a\*</sup>, Sarvia F.<sup>a</sup>, Borgogno-Mondino E.<sup>a</sup>

<sup>a</sup>Department of Agriculture, Forestry and Food Sciences, University of Torino, Grugliasco (TO), 10095, Italy

\*Corresponding author: samuele.depetris@unio.it

Commission III, WG III/7

**KEY WORDS:** Sentinel-1, SAR, Forest Harvestings Detection, Cross Ratio index, Time series analysis.

## ABSTRACT:

Satellite remote sensing has long been used to monitor forest harvesting with accuracies appropriate for practical mapping across a wide range of forest types by using different sensors. Unfortunately, in Italy, most of the cuts take place in winter where the cloud cover is very high, making it impossible an early detection by optical data. In this framework, synthetic aperture radar (SAR) data such as Sentinel-1 (S1) allows a better land monitoring by penetrating cloud cover. In this work we tested some methods for time series breakpoint detection with the aim of mapping significant forest cover changes in 2019 over an Italian forested area. These maps can be useful tools to support the focusing of field surveys by forest police with the aim of increasing the monitorable areas and decreasing the related field survey costs. Four methods were proposed and compared based on the analysis of SAR polarimetric index time series (Cross Ratio index). In particular, adopted methods search for a breakpoint in the cross-ratio time series assuming it as moment after that forest canopy temporal behaviour significantly change. In general, high overall accuracy and user's accuracy were found for all methods while producer's accuracy and K values are lower denoting an underestimation of harvested areas by single method. Conversely, combining all methods into a final classification shows highest user's accuracy (> 0.9) in detecting forests harvestings when more than two classification methods were adopted.

## 1. INTRODUCTION

Remote sensing is well-known for its effectiveness in detecting and interpreting forest changes. Satellite remote sensing has long been used to monitor forest harvesting with accuracies appropriate for practical mapping across a wide range of forest types and sensors. Many studies adopted optical remote sensing for detecting forest cover changes (Gao et al., 2020; Heckel et al., 2020; Lui and Coomes, 2015; Singh, 1989) since spaceborne remotely sensed data is less expensive than data from other sources (Holmgren and Thuresson, 1998). Despite the widespread use of optical data for estimating forest harvestings (De Petris et al., 2020; Hall et al., 1989; Saksa et al., 2003), this type of sensing is restricted by sun irradiation and cloud covering. Especially the latter condition affects the availability of images over tropical/equatorial forests that are known to be the most illegally harvested forests (Reiche et al., 2016). Also European forests are very harvested (Levers et al., 2014) and this issue is very cared by public opinion (Rametsteiner and Kraxner, 2003; Ranacher et al., 2020) therefore many European countries enact laws to restrict forest harvesting intensity. In Italy harvesting's location and expected timber removal must be communicated before the intervention and bigger cuts need a formal permission by forestry authority. Illegal harvestings monitoring must be performed by local Forest police. Ordinarily, police checks are performed by a notice or by ground controls sampling (about 5% of communications) comparing the intervention features in respect to forest regulation. Unfortunately, this procedure does not allow a land synoptic monitoring, leaving unchecked the 95% of the requests and illegal harvestings could be not detected. In this context, remote sensing offers a major monitoring capability than the one based on ground checks. Thus, forest harvesting monitoring services based on earth observation imagery (e.g. Copernicus programme) are growing (De Petris et al., 2020). Unfortunately, in Italy, most of the cuts take place in winter

where the cloud cover is very high, making it impossible an early detection by optical data. In this framework, synthetic aperture radar (SAR) data such as Sentinel-1 (S1) allows a better land monitoring by penetrating cloud cover (Geudtner et al., 2014). In addition, SAR data are more sensitive to the surfaces geometric properties potentially allowing significant changes detection in vegetation cover induced by trees removal (Askne and Santoro, 2005). In this work we tested some change detection methods with the aim of detecting significant changes in forest cover and producing maps useful for detecting these areas. These can be useful tools to support the focusing of field surveys by forest police with the aim of increasing the monitorable areas and decreasing the related field survey costs.

## 2. MATERIALS

### 2.1 Study Area

The area of interest (AOI) sizes about 96 km<sup>2</sup> and it is placed in the North of the Piemonte region (NW - Italy). AOI is characterised by a dominant presence of forest (about 70%) and an altitudinal range between 250 and 800 m a.s.l (Fig.1). In addition, AOI is noted for having numerous requests for forestry cuts, which makes it an excellent and interesting area for the aims of this work. It is worth to remind that winter is the silvicultural season in Piemonte. In particular, allowed harvesting period starts on 1<sup>st</sup> October and ends on 31<sup>st</sup> May. In this work, 2019 was selected as reference period for testing our methods.

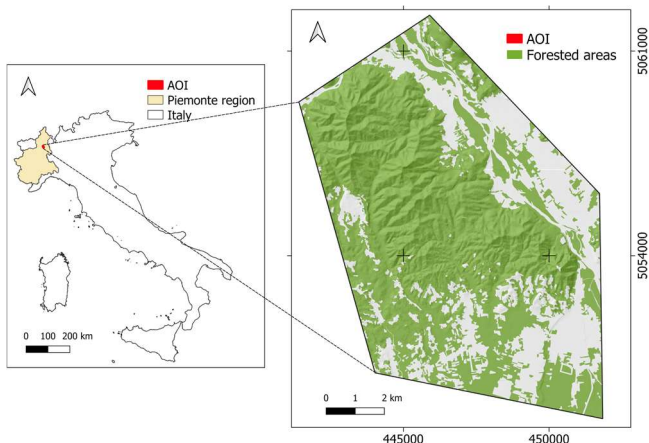


**Figure 1.** AOI location. Reference frame is WGS84 UTM 32N.

## 2.2 Available data

The difficulty of SAR data pre-processing, according to Vollrath (Vollrath et al., 2020) and Reiche (Reiche et al., 2016) is one of the key reasons for its slowly adoption by a larger user community. In this regard, the Google Earth Engine (GEE) web-based platform provides instant access to SAR imagery and allows users to focus on the information they need (Gorelick et al., 2017) making such data provider useful to transfer the following approach into operative framework. Therefore, in this work, satellite imagery was collected using GEE while others data were download from free-available database.

**2.2.1 Forest map:** The forestry map (FM) of the Piemonte Region (Camerano et al., 2017), was used to identify forest areas within AOI. FM has a nominal scale of 1:10000 and updated in 2016. It was obtained freely as a vector layer from the regional geoportal ([www.geoportale.piemonte.it](http://www.geoportale.piemonte.it)).

**2.2.2 Sentinel-1 imagery:** S1 ground range detected (GRD) IW (Interferometric Wide Swath) image collection, available in Google Earth Engine (GEE), was used. S1 GRD products consist of focused, detected, multi-looked SAR data projected to ground range. The product has an approximately squared pixel with a spatial resolution of about 10 m provided in backscattering values (dB) for VV and VH polarizations. All images in the period 1<sup>st</sup> June 2018 and 30<sup>th</sup> June 2020 were considered for two orbits: orbit path = 66 for ascending and orbit path = 88 for descending. A total of 120 images were analysed. This sensing period was selected to fit the silvicultural season in Piemonte. Considering the 2019 silvicultural season, two winters can occur, one between 2018-2019 and the other between 2019-2020. Therefore, starting from summer 2018 until summer 2020 should assure a proper times series length to detect harvestings in 2019. In order to minimize speckle all images were averaged at the monthly level generating a S1 time series having 24 images for each polarization and orbit. Since AOI is in mountain area, some geometric distortions are expected to negatively affect the monitorability of forest cover (Chen et al., 2018). Unfortunately, GEE S1 imagery currently has not a mask accounting for distortion mapping. Therefore, two S1 GRD images were download from Copernicus SciHub (<https://scihub.copernicus.eu/>); one was acquired on 21<sup>st</sup> of November 2021 for the ascending orbit (orbit path = 66) the other was acquired on 2<sup>nd</sup> December 2021 for descending orbit (orbit path = 88) and were processed in SNAP vs 8.0 (Veci et al., 2014) to map geometric distortions.

**2.2.3 Reference data:** A total of 24 reference data (RD) were acquired to validate the methodological approach suggested in this work (Fig. 2). RD was collected by photointerpretation of a couple of orthophotos (having a geometrical resolution of 30 cm) available in Google Earth Pro imagery. Specifically, the images referring to August 2018 and September 2019 were used in order to detect significant variations associated with forest cuts in the forest pattern within AOI. Subsequently, area delimitation was carried out by polygons drawing, resulting in a vector file containing all RD patches. In particular, 8 patches were identified as not harvested (about 30.7 ha) and 16 as harvested (about 9.8 ha).

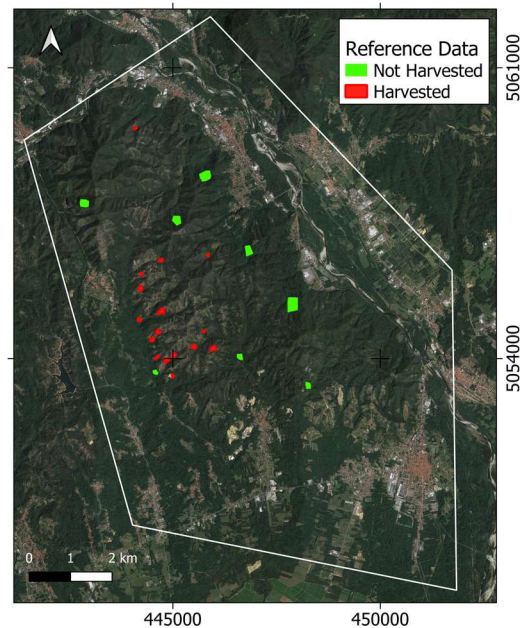


**Figure 2.** Harvested and not-harvested reference polygons location in AOI. Reference frame is WGS84 UTM 32N.

## 3. METHODS

### 3.1 CR time series generation

In this work, the Cross-ratio (CR) radar index was adopted to monitor forest canopy. In fact, CR is sensitive to vegetation canopy density (Vreugdenhil et al., 2020), therefore a canopy structure change should affect CR values (De Petris et al., 2021; Mandal et al., 2020; Nasirzadehdizaji et al., 2019). CR was computed directly on GEE by subtraction between S1 VH and VV time series previously defined (i.e.  $CR_{dB} = VH_{dB} - VV_{dB}$ ), resulting in 2 different CR time series (CRTS) having 24 observations, one for ascending orbit and one for descending one. Subsequently, the two CR stacks were downloaded and projected into the WGS84/UTM 32N (EPSG: 32632) reference frame.

### 3.2 SAR geometric distortions masks

Considering many SAR images acquired from the same orbit path, look angle for the same pixel does not change significantly along the CRTS, therefore, parallel rays' approximation commonly used in interferometry could be assumed (Richards, 2009) and SAR geometric distortion should be in the same position along the analysed period. Hence, only two S1 GRD images were used in this work to detect SAR geometric distortions. The latter were mapped using the tool available in SNAP. Specifically, layover and shadows areas were detected using orbit information and SRTM HGT digital elevation model

having a geometric resolution of 30 m. Finally, distortions were then geocoded into WGS84 UTM 32N reference frame for both ascending and descending images. Resulted images were used to mask out all CRTS pixels in the distorted areas.

### 3.3 Harvesting's detection methods

In this work, 4 different methods for forest harvesting detection were used and compared. All methods are based on the assumption that a forest harvesting constitutes a single breakpoint in the CRTS significantly changing CR behaviour after the event moving from higher CR values to lower ones. All breakpoint analysis were performed using *R software vs 4.1* (R Development Core Team, 2013).

**3.3.1 Pettitt's test:** The Pettitt's test is a non-parametric test based on Mann-Whitney two sample test (rank based) (Pettitt, 1979) that looks for a single breakpoint at an unknown observation  $t$ . The null hypothesis is that no change occurs along the CRTS; the alternative hypothesis is that the CRTS built in the range before  $t$  is significantly different from the one built after the breakpoint. If the corresponding  $p$ -value is lower than the selected significance level, one can reject the null hypothesis; consequently, the CRTS can be divided into two sub-series. The map of breakpoint moment (i.e. CRTS observation at which occurred a significant breakpoint) and the map of correspondent  $p$ -value were computed maintaining the same geometrical resolution of CRTS. In this work, the significance level was cauteratively set equal to 0.9 ( $\alpha = 0.1$ ). Therefore, all pixels having  $p$ -value greater than 0.1 were masked out, while the reminder ones were coded as 1 and labelled as Harvested.

**3.3.2 Residuals CUSUM:** This method is based on the cumulative sum of the residuals of the differences between CRTS and the mean of CRTS signal in the considered period. The CUSUM function is increasing before the breakpoint and starts decreasing after the breakpoint; therefore, the moment at CUSUM is maximized can be assumed as the breakpoint one and mapped accordingly. Unfortunately, for each CRTS profile a maximum is always possible, therefore an auxiliary statistic hereafter called SD (Significance of the difference) was computed and mapped according to eq.1.  $SD(x,y)$  map can be used to assess if the difference between two mean signals, i.e. before and after the breakpoint, is significant based on variance propagation law (Hughes and Hase, 2010). Assuming the standard error of the mean (SEM) as a measure of the mean uncertainty (Andrade, 2020) we can compute the uncertainty of the difference and compare it (by ratio) to the difference value. SD value greater than 1 means that signal difference before and after the breakpoint is significantly higher than its uncertainty (i.e noise). Cauteratively, this significance was set double (i.e. 2) in order to guarantee a better detection of highly significant breakpoints.

$$SD(x, y) = \frac{\mu_{1:t} - \mu_{t:24}}{\sqrt{(SEM_{1:t})^2 + (SEM_{t:24})^2}} \quad (1)$$

Where  $\mu_{1:t}$  and  $\mu_{t:24}$  are mean CR signals before and after the breakpoint respectively considering 24 observations in CRTS.  $SEM_{1:t}$  and  $SEM_{t:24}$  are the standard errors of the mean before and after the breakpoint respectively. The pixels having SD lower than 2 were masked out, while the reminder ones were coded as 1 and labelled as Harvested.

**3.3.3 Linear trend slope:** A third approach to detect forest harvestings is based on the assumption that harvested forest pixels have a negative trend since they move from higher CR values to lower ones with no significant recovery rate in the considered period (two years). Thus, the trend was modelled as first order polynomial by ordinary least squares between CR values and observations time at the pixel level. Subsequently, the slope value and its significance, i.e.  $p$ -value of t-test to assess that slope value is significantly different from 0 (Andrade and Estévez-Pérez, 2014), were mapped. All pixels having a  $p$ -value higher than 0.1 or having a positive slope value were masked out, while the reminder ones were coded as 1 and labelled as Harvested.

**3.3.4 Three methods combination:** To give a degree of reliability of the detections about harvested areas, a final classification was produced combining the previously mentioned methods. In particular, the three harvestings' classifications were summed resulting in a new map with the following codes: 0, for not harvested forests; 1, for those pixels having at least one classification coded as 1 (harvested); 2, for those pixels having at least two classifications coded as 1 (harvested); 3, for those pixels having all classifications coded as 1 (harvested).

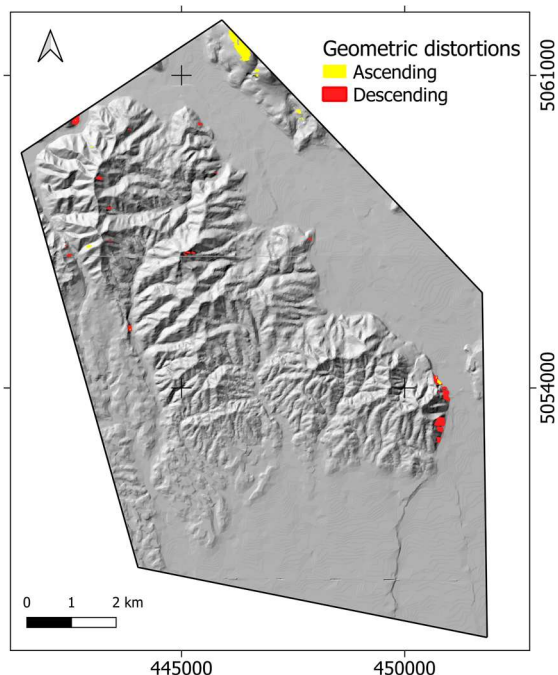
### 3.4 Validation and comparison

All methods were assessed by confusion matrix computation involving RD. In particular, producer's accuracy (PA), user's accuracy (UA), overall accuracy (OA) and kappa values (K) were computed according to (Congalton and Green, 2019) for each classification and for both ascending and descending orbits.

## 4. RESULTS AND DISCUSSIONS

### 4.1 SAR geometric distortions masks

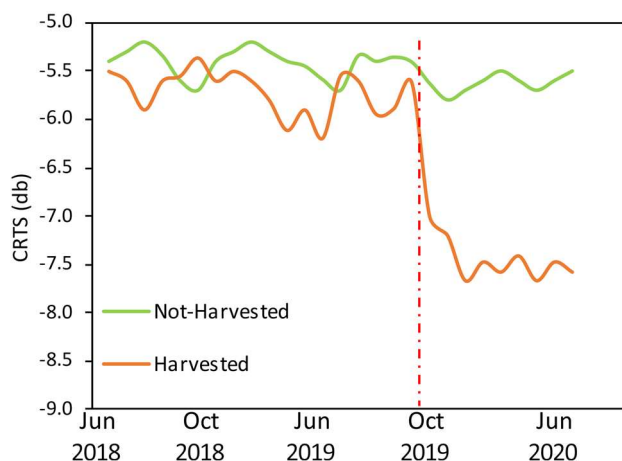
Using SNAP software, the geometric distortions were mapped (Fig. 3) and related CRTS pixels finally masked out from subsequently processing steps. About 21 ha and 17 ha were detected as distorted areas for ascending and descending images respectively, denoting how less than 1% of the forest areas were distorted. This analysis shows that ascending orbit see more than 23% of distorted areas than descending orbit highlighting how ascending CRTS has a minor monitoring capability than descending one in AOI.



**Figure 3.** Geometric distortions mapped by SNAP tool for ascending and descending nodes. Reference frame is WGS84 UTM 32N.

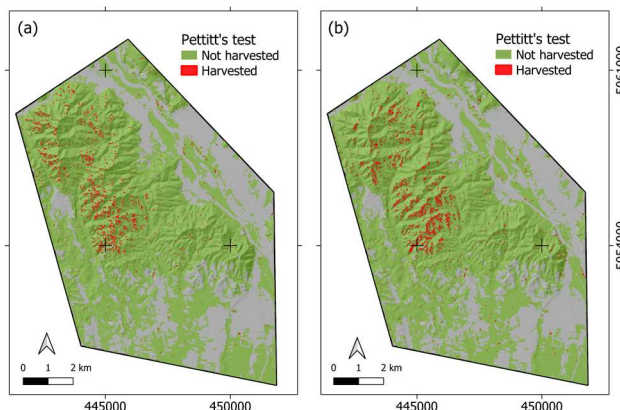
#### 4.2 Harvesting's detection methods

Figure 4 shows CRTS profiles representing the average CR values of RD for both harvested and not-harvested areas. After October 2019 there is a clear decreasing of CR values probably caused by forest harvesting in AOI. This moment could be assumed as CRTS breakpoint. In fact, before this moment CRTS are very similar for both RD classes; after breakpoint CRTS profiles show different behaviours. RD harvested areas have lower CR values than not-harvested ones, supporting the hypothesis that forest harvesting significantly change vegetation structure/cover resulting into different CRTS.



**Figure 4.** CRST average profiles of RD. Red line is the expected winter cutting moment considering the 2019 silvicultural season.

The forest harvestings detection map using the Pettitt's test approach is reported in figure 5. Adopting this method, about 208 ha and 239 ha were classified as harvested for in the 2019.



**Figure 5.** Forest harvestings classification by Pettitt's test method for (a) ascending CRTS and (b) for descending CRTS. Reference frame is WGS84 UTM 32N.

The forest harvestings detection map using the residuals CUSUM approach is reported in figure 6. Adopting this method, about 828 ha and 737 ha were classified as harvested for in the 2019.

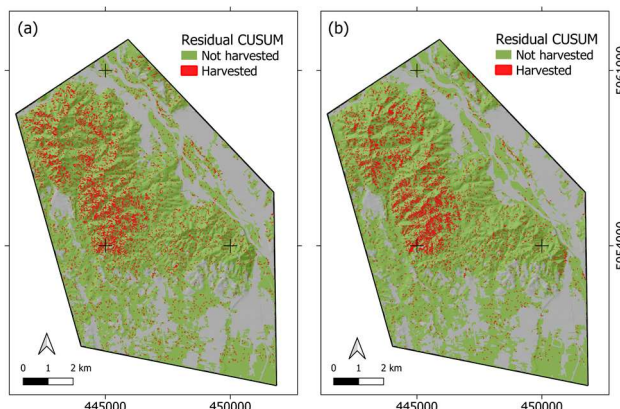


**Figure 6.** Forest harvestings classification by Residuals CUSUM method for (a) ascending CRTS and (b) for descending CRTS. Reference frame is WGS84 UTM 32N.

The forest harvestings detection map using the linear trend slope approach is reported in figure 7. Adopting this method, about 296 ha and 272 ha were classified as harvested for in the 2019.

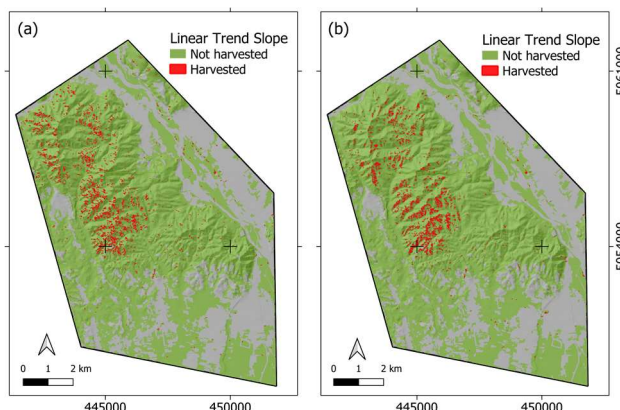


**Figure 7.** Forest harvestings classification by Linear Trend Slope method for (a) ascending CRTS and (b) for descending CRTS. Reference frame is WGS84 UTM 32N.

The forest harvestings detection map using the combined approach is reported in figure 8. Adopting this method and assuming harvested all pixels having a value greater than equal to 1, about 704 ha and 651 ha were classified as harvested for in the 2019. In particular, for both ascending and descending nodes about 25% of harvested pixels were coded as harvested (3); about 10% for harvested (2) while 65% as harvested (1).

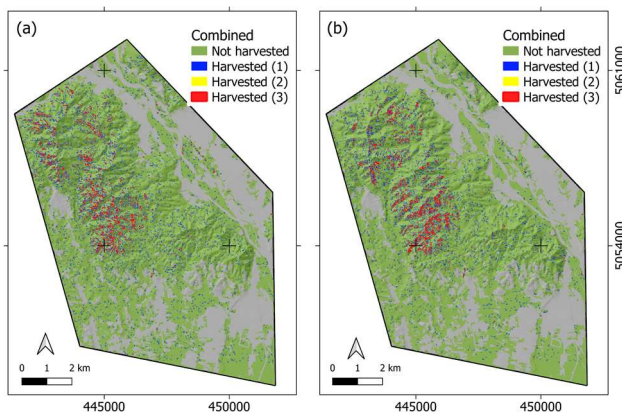


**Figure 8.** Forest harvestings classification by combined method for (a) ascending CRTS and (b) for descending CRTS. Colours represent how many times a pixel was classified as Harvested by combining all methods. Reference frame is WGS84 UTM 32N.

In general, it can be noted that ascending orbit overestimates of about 10% than descending one for all methods excepting for Pettitt's test approach where harvesting classification by ascending imagery underestimates of about 12% than descending orbit.

### 4.3 Validation and comparison

Proposed methods accuracies were computed in respect to RD using confusion matrix elements. Figure 9 reports the OA and K values for each classification. In general, all classifications have OA greater than 0.78 for ascending orbit while OA greater than 0.85 for descending one with no significant differences between methods. K values are higher in descending ( $>0.59$ ) than ascending ( $>0.34$ ) denoting a major randomness contribution for ascending classifications.

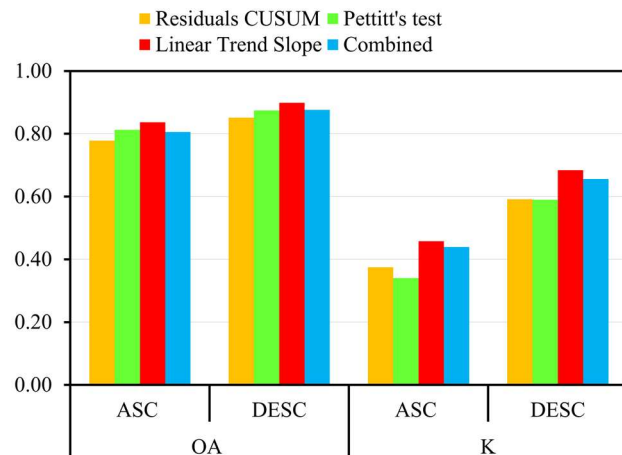


**Figure 9.** OA and K values resulting from different forest harvesting classifications in respect to RD.

PA values reported in Figure 10a, appear to be quite high for Not-Harvested class for both ascending ( $PA > 0.87$ ) and descending orbit ( $PA > 0.91$ ). For this class no significant differences in PA between methods were found. Conversely, some critical points were found in the Harvested class. Specifically, a great difference between ascending and descending orbit was noted resulted in  $PA > 0.28$  and  $PA > 0.50$  respectively. Moreover, significant PA differences between methods have been observed. In particular, Pettitt's test was the worst performing method, while the combined method results to be the best having PA equal to 0.52 and 0.72 for ascending and descending orbits respectively. UA values reported in Figure 10b, appear to be quite high for Not-Harvested class for both ascending and descending orbit,  $UA > 0.81$  and  $UA > 0.86$  respectively. For this class no significant differences in UA between methods were found. While, again, some critical points were found in the Harvested class. Specifically, a great difference between ascending and descending orbit was noted,  $UA > 0.55$  and  $UA > 0.76$  respectively. Moreover, significant UA differences between methods have been observed. In particular, Residuals CUSUM was the worst performing method, while Pettitt's test (UA equal to 0.83 and 0.97 for ascending and descending orbit respectively) and Linear Trend Slope (UA equal to 0.84 and 0.96 for ascending and descending orbit respectively) prove to be the best methods. Combined method shows UA equal to 0.62 and 0.76 for the ascending and descending orbit respectively.

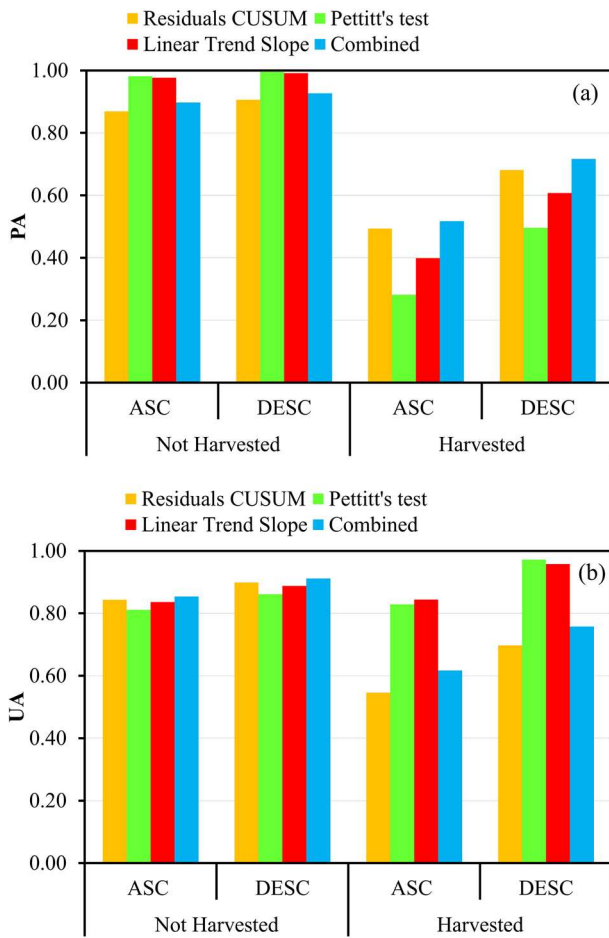


**Figure 10.** (a) PA and (b) UA values resulting from different forest harvesting classifications in respect to RD.

Unfortunately, all classifications show medium-low PA values for harvested areas denoting a general underestimation of harvestings. Nevertheless, UA values show medium-high accuracy denoting that detected harvestings are effectively mapped. Considering this discrepancy, it is desirable to select a method that balances PA and UA. Therefore, in this context the combined method appears to be a good compromise. Specifically, it should be noted that the descending orbit showed excellent results for both Not Harvested class, UA equal to 0.91, PA equal to 0.93, and Harvested class UA equal to 0.76, PA equal to 0.72, resulting in an OA equal to 0.81. It is worth to remind that in a technology transfer context, where detection and monitoring of forest cuts could be carried out by S1 data, the use of combined method allows the forest authority to obtain a map of reliability degree of the deductions from harvesting detection map. In particular, the combined method gives us information about the concordance between other proposed methods, counting how many times a forest pixel is seen harvested by different methods. From figure 11 it can be noted that pixels coded as harvested (1), i.e. classified as harvested by only one method, show very low UA values ( $< 0.52$ ) for both ascending and descending orbits, while considering class harvested (2) and harvested (3) show very high UA values  $> 0.90$  for descending. These results suggest that if more than two harvesting detection methods are adopted, combined classification is very accurate and prove to be an effective procedure. Despite these results, some doubts still persist concerning the discrepancy between classifications generated by ascending and descending CRTS. In fact, CR index should allow to compare images acquired from

slightly different look angle (De Petris et al., 2021), but the consistency seems not so effective resulting into different CRTS behaviours and finally generating harvesting different detection results. A possible reason of this discrepancy could be the presence of not modelled geometric distortions as mapped by SNAP software. A recent work developed by (De Petris et al., 2021) proved how slightly changes of look angle from images taken from the same orbit path can negatively affect target-sensor line of sight visibility. Probably, the jointly adoption of a coarse resolution DEM (i.e. SRTM) and not considering the active/passive relationship between layover/shadows areas from SNAP tool, compromised the effectiveness of geometric distortion mapping. Further experiments will be expected to prove this hypothesis adopting the routine developed by (De Petris et al., 2021) directly applicable in GEE.

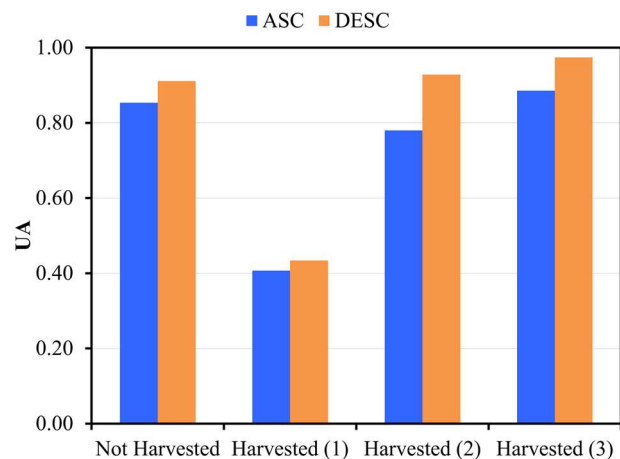


**Figure 11.** UA values of different classes in the combined method using ascending and descending CRTS.

## 5. CONCLUSIONS

In this work different methods to detect forest harvestings were compared. All methods are based on the analysis of SAR polarimetric index time series (i.e., CR). In particular, adopted methods search for a breakpoint in the CRTS assuming it as moment after that forest canopy temporal behaviour significantly change. In general, high OA and UA were found for all methods while PA and K values are lower denoting a underestimation of harvested areas by single method. Conversely, the combined method shows highest UA accuracy ( $> 0.9$ ) when more than two classification method were adopted.

In respect of more common supervised classification methods (like machine learning ones), the adoption of time series analysis approach allows to be independent from a training data making these approach more transferable to operative sector. Moreover, the combined method here proposed allows mapping how many times a pixel is seen as harvested by different classifiers alerting the final user (i.e. forest police) about the reliability degree of the deductions from S1 imagery. Finally, some doubt about the discrepancy between deductions derived by CRTS from ascending and descending nodes have been raised opening new research scenarios to investigate this phenomenon.

## REFERENCES

Andrade, C., 2020. Understanding the difference between standard deviation and standard error of the mean, and knowing when to use which. *Indian Journal of Psychological Medicine* 42, 409–410.

- Andrade, J.M., Estévez-Pérez, M.G., 2014. Statistical comparison of the slopes of two regression lines: A tutorial. *Analytica chimica acta* 838, 1–12.
- Askne, J., Santoro, M., 2005. Multitemporal repeat pass SAR interferometry of boreal forests. *IEEE Transactions on Geoscience and Remote Sensing* 43, 1219–1228.
- Camerano, P., Terzuolo, P.G., Guiot, E., Giannetti, F., 2017. La Carta Forestale del Piemonte – Aggiornamento 2016. IPLA S.p.A. – Regione Piemonte.
- Chen, X., Sun, Q., Hu, J., 2018. Generation of complete SAR geometric distortion maps based on DEM and neighbor gradient algorithm. *Applied Sciences* 8, 2206.
- Congalton, R.G., Green, K., 2019. Assessing the accuracy of remotely sensed data: principles and practices. CRC press.
- De Petris, S., Berretti, R., Guiot, E., Giannetti, F., Motta, R., Borgogno-Mondino, E., 2020. Detection And Characterization of Forest Harvesting In Piedmont Through Sentinel-2 Imagery: A Methodological Proposal. *Annals of Silvicultural Research* 45, 92–98. <https://doi.org/10.12899/asr-2018>
- De Petris, Samuele, Sarvia, F., Gullino, M., Tarantino, E., Borgogno-Mondino, E., 2021. Sentinel-1 Polarimetry to Map Apple Orchard Damage after a Storm. *Remote Sensing* 13, 1030.
- De Petris, S., Sarvia, F., Orusa, Borgogno-Mondino, E., 2021. Mapping SAR geometric distortions and their stability along time: a new tool in Google Earth Engine based on Sentinel-1 image time series. *International Journal of Remote Sensing* 42, 9135–9154. <https://doi.org/10.1080/01431161.2021.1992035>
- Gao, Y., Skutsch, M., Paneque-Gálvez, J., Ghilardi, A., 2020. Remote sensing of forest degradation: a review. *Environmental Research Letters* 15, 103001.
- Geudtner, D., Torres, R., Snoeij, P., Davidson, M., Rommen, B., 2014. Sentinel-1 system capabilities and applications, in: 2014 *IEEE Geoscience and Remote Sensing Symposium*. IEEE, pp. 1457–1460.
- Gorelick, N., Hancher, M., Dixon, M., Ilyushchenko, S., Thau, D., Moore, R., 2017. Google Earth Engine: Planetary-scale geospatial analysis for everyone. *Remote sensing of Environment* 202, 18–27.
- Hall, R.J., Kruger, A.R., Moore, W.C., Scheffer, J., Titus, S.J., 1989. A statistical evaluation of Landsat TM and MSS data for mapping forest cutovers. *The Forestry Chronicle* 65, 441–449.
- Heckel, K., Urban, M., Schratz, P., Mahecha, M.D., Schmullius, C., 2020. Predicting forest cover in distinct ecosystems: The potential of multi-source Sentinel-1 and-2 data fusion. *Remote Sensing* 12, 302.
- Holmgren, P., Thuresson, T., 1998. Satellite remote sensing for forestry planning—A review. *Scandinavian Journal of Forest Research* 13, 90–110. <https://doi.org/10.1080/02827589809382966>
- Hughes, I., Hase, T., 2010. Measurements and their uncertainties: a practical guide to modern error analysis. OUP Oxford.
- Levers, C., Verkerk, P.J., Müller, D., Verburg, P.H., Butsic, V., Leitão, P.J., Lindner, M., Kuemmerle, T., 2014. Drivers of forest harvesting intensity patterns in Europe. *Forest Ecology and Management* 315, 160–172.
- Lui, G.V., Coomes, D.A., 2015. A comparison of novel optical remote sensing-based technologies for forest-cover/change monitoring. *Remote Sensing* 7, 2781–2807.
- Mandal, D., Kumar, V., Ratha, D., Dey, S., Bhattacharya, A., Lopez-Sanchez, J.M., McNairn, H., Rao, Y.S., 2020. Dual polarimetric radar vegetation index for crop growth monitoring using sentinel-1 SAR data. *Remote Sensing of Environment* 247, 111954.
- Nasirzadehdizaji, R., Balik Sanli, F., Abdikan, S., Cakir, Z., Sekertekin, A., Ustuner, M., 2019. Sensitivity analysis of multi-temporal Sentinel-1 SAR parameters to crop height and canopy coverage. *Applied Sciences* 9, 655.
- Pettitt, A.N., 1979. A non-parametric approach to the change-point problem. *Journal of the Royal Statistical Society: Series C (Applied Statistics)* 28, 126–135.
- R Development Core Team, R., 2013. R: A language and environment for statistical computing. R foundation for statistical computing Vienna, Austria.
- Rametsteiner, E., Kraxner, F., 2003. Europeans and their forests. What do Europeans think about forests and sustainable forest management.
- Ranacher, L., Sedmik, A., Schwarzbauer, P., 2020. Public perceptions of forestry and the forest-based bioeconomy in the European Union. EFI Knowledge to Action; European Forest Institute: Joensuu, Finland.
- Reiche, J., Lucas, R., Mitchell, A.L., Verbesselt, J., Hoekman, D.H., Haarpaintner, J., Kellndorfer, J.M., Rosenqvist, A., Lehmann, E.A., Woodcock, C.E., 2016. Combining satellite data for better tropical forest monitoring. *Nature Climate Change* 6, 120–122.
- Richards, J.A., 2009. Remote sensing with imaging radar. Springer.
- Saksa, T., Uuttera, J., Kolström, T., Lehikoinen, M., Pekkarinen, A., Sarvi, V., 2003. Clear-cut Detection in Boreal Forest Aided by Remote Sensing. *Scandinavian Journal of Forest Research* 18, 537–546. <https://doi.org/10.1080/02827580310016881>
- Singh, A., 1989. Review article digital change detection techniques using remotely-sensed data. *International journal of remote sensing* 10, 989–1003.
- Veci, L., Prats-Iraola, P., Scheiber, R., Collard, F., Fomferra, N., Engdahl, M., 2014. The sentinel-1 toolbox, in: *Proceedings of the IEEE International Geoscience and Remote Sensing Symposium (IGARSS)*. IEEE, pp. 1–3.
- Vollrath, A., Mullissa, A., Reiche, J., 2020. Angular-Based Radiometric Slope Correction for Sentinel-1 on Google Earth Engine. *Remote Sensing* 12, 1867.
- Vreugdenhil, M., Navacchi, C., Bauer-Marschallinger, B., Hahn, S., Steele-Dunne, S., Pfeil, I., Dorigo, W., Wagner, W., 2020.

Sentinel-1 cross ratio and vegetation optical depth: A comparison over Europe. *Remote Sensing* 12, 3404.